

Heavy systems at intermediate energies in the Boltzmann-Uehling-Uhlenbeck approach

J. Aichelin*

*Joint Institute for Heavy Ion Research, Holifield Heavy Ion Research Facility, Oak Ridge, Tennessee 37831
and Physics Division, Oak Ridge National Laboratory, Oak Ridge, Tennessee 37831*

(Received 7 June 1985)

The Boltzmann-Uehling-Uhlenbeck equation is applied to nucleus-nucleus collisions with heavy targets, extending previous work on light systems. The model exhibits a hot source of nonequibrated particles, giving single-particle spectra that are in reasonable agreement with experiment for the case studied, $84A$ MeV $^{12}\text{C} + ^{197}\text{Au}$. However, the source is not localized in space, which questions the validity of models using global or local thermal equilibrium. The equilibration of the heavy remnant is not completed by 180 fm/ c and turns out to be a complicated interplay between the mean field and collisions. The projectile transfers nearly all of its linear momentum to the target for energies up to $30A$ MeV. At higher energies the linear momentum transfer is incomplete, even for central collisions.

I. INTRODUCTION

Recently numerical solutions of the Boltzmann-Uehling-Uhlenbeck (BUU) equation were advanced.¹ This equation describes the time evolution of the one-body phase space distribution under the influence of a self-consistent mean field and hard core collisions which obey the Pauli principle. They were used to describe intermediate energy heavy ion collisions in the energy range between $25A$ and $150A$ MeV.² In this energy domain the one-body and two-body dynamics are of comparable importance. Hence time dependent Hartree-Fock (TDHF) calculations, which include only the one-body dynamics, fail as well as high energy intranuclear cascade (INC) calculations, which contain only the two-body dynamics.

We applied this model to simulate the reactions $25A$ MeV $^{16}\text{O} + ^{12}\text{C}$ and $84A$ MeV $^{12}\text{C} + ^{12}\text{C}$.² Comparison with the experimental proton spectra showed a good agreement in the absolute magnitude as well as in shape. Furthermore we observed that the $25A$ MeV reaction resembles the typical low energy phenomena like fusion and deep inelastic processes which are accompanied by a preequilibrium emission in longitudinal direction. The $84A$ MeV reaction on the other hand fits well in the observed high energy phenomenology. We saw that the emitted particles come predominantly from the geometrical overlapping zone which develops into a midrapidity source. This resembles the participant-spectator model.

However, the smallness of the targets did not allow us to address some important questions. Phenomenological models of reactions with heavy targets describe the data quite well assuming that the evaporated particles come predominantly from a hot localized source which contains only part of the target nucleons.^{3,4} From geometrical considerations this hot spot should emit particles into the backward direction but the preequilibrium particles are seen mainly in the forward direction. How can this be reconciled?

Another issue is raised by experiments that observe substantial numbers of heavy fragments ($4 < A < 20$), seen at

energies as low as $35A$ MeV in $^{12}\text{C} + ^{197}\text{Au}$ reactions.⁵ The explanations for this process range from cold fragmentation to the speculation that the system undergoes a phase transition.⁶⁻⁸ Although the restriction to the one-body phase space density does not allow us to address the emission of heavy fragments in a direct way, it enables us to investigate whether or how the system equilibrizes, a necessary condition for the applicability of thermal models.

At low energy the projectile transfers its total available momentum to the compound nucleus (complete fusion). With increasing beam energy the transfer gets less complete.⁹ This process has been named incomplete fusion but did not get a proper description in physical terms. It is not known whether this can be reduced to a geometrical effect; i.e., whether only the geometrically overlapping projectile nucleons transfer momentum to the target or whether the target gets increasingly transparent with increasing energy.

To address these questions we performed simulations for a variety of systems chosen to allow comparison with available data. In Sec. II we summarize our numerical technique. To prove whether our method works for larger targets as well we investigate in detail the reaction $84A$ MeV $^{12}\text{C} + ^{197}\text{Au}$, where two independent sets of single particle spectra have been measured by Jakobsson *et al.*¹⁰ and Santo *et al.*¹¹ A survey of the time evolution of this reaction is given in Sec. III, the detailed results as well as the comparison with data are presented in Sec. VI. In Sec. IV we study the question whether a hot localized subsystem can be found in intermediate heavy ion reactions by means of low impact parameter calculations for the systems $25A$ MeV, $250A$ MeV $^{16}\text{O} + ^{197}\text{Au}$, and $84A$ MeV $^{12}\text{C} + ^{197}\text{Au}$. In Sec. V we investigate the thermalization of the heavy remnant.

In Sec. VI we present the experimental observables of our calculations. These include fusion cross sections, single particle spectra, multiplicity distributions of the evaporated particles, the distribution of the linear momentum transfer, and the out of plane correlations. We com-

pare the calculations with the single particle spectra by Jakobsson *et al.*¹⁰ and Santo *et al.*¹¹ for the reaction $84A$ MeV $^{12}\text{C} + ^{197}\text{Au}$, the measurements of Galin *et al.*¹² on the linear momentum transfer for $30A$, $60A$, and $84A$ MeV $^{12}\text{C} + ^{197}\text{Au}$, and the azimuthal correlation at $25A$ MeV $^{16}\text{O} + ^{197}\text{Au}$ of Tsang *et al.*¹³ This section contains also a systematic study of the target mass dependence of the linear momentum transfer in low impact parameter reactions $84A$ MeV $^{12}\text{C} + A$ and $44A$ MeV $^{40}\text{Ar} + A$.

Finally in Sec. VII we present our conclusions.

II. BUU EQUATION

For the derivation of the BUU equation the reader is referred to Refs. 14 and 15. The equation describes the time evolution of the single particle phase space distribution $f(p, r)$ in a self-consistent mean field U and reads as follows:

$$\begin{aligned} \frac{\partial f_1}{\partial t} + v \cdot \nabla_r f_1 - \nabla_r U \cdot \nabla_p f_1 \\ = - \int \frac{d^3 p_2 d^3 p_1' d^3 p_2'}{(2\pi)^9} \sigma v_{12} [f_{1,2}(1-f_{1'}) (1-f_{2'}) - f_{1,2'}(1-f_1)(1-f_2)] (2\pi)^3 \delta^3(\mathbf{p} + \mathbf{p}_2 - \mathbf{p}_1' - \mathbf{p}_2') . \end{aligned}$$

In our calculation this equation is slightly modified. We do not use the stosszahlansatz $f_1 f_2$ but the two-body density which is given automatically by the time evolution of our classical $N_T + N_P$ Liouville equation.² However, our phase space distribution is essentially a classical distribution of particles with sharp momenta and positions and we are not able to treat quantum mechanical correlations correctly. Furthermore the correlations get disturbed by calculating 100 simulations in parallel.² Hence from a practical point of view this difference may be neglected.

At energies as low as $25A$ MeV it is essential to treat the antisymmetrization properly. This is done by the choice of the initial condition: initially the nucleons are placed in a sphere with the radius of the nucleus. Then a random momentum is assigned to each nucleon whose maximum is given by a local Fermi gas approximation. Finally we boost the nuclei towards each other. This description guarantees that the Pauli principle is fulfilled initially in the average although it is only a mockup for the antisymmetrization. As the very similar time evolution of the TDHF and the Vlasov calculation² show, this approximation mocks up the antisymmetrization during the whole course of the nuclear reaction.

Until the beginning of the nucleon-nucleon collisions projectile and target are moved on Coulomb trajectories. In the further time evolution of the system we neglect this long range force, since we are primarily interested in the preequilibrium processes. Only for particles emitted with an energy near the Coulomb barrier we expect larger uncertainties due to these approximations. However, those particles come predominantly from the late stage of the reaction when the system is close to equilibrium. For details of the numerical simulation we refer the reader to Ref. 2. Up to $84A$ MeV we use nonrelativistic kinematics.

III. APPLICATION TO HEAVY SYSTEMS

As we have shown, the BUU equation predicts well the experimental observables for light system. The application to heavier targets, however, is more demanding. For the same bombarding energy we have to ensure the stability of the system for a large time duration needed to com-

plete the reaction. Also the computing time raises nonlinearly. Whereas the mean field part is proportional to the number of test particles (N) the collision part is proportional to N^2 . Currently 8 h CPU time on an FPS system are required for 100 simulations of the system $^{12}\text{C} + ^{197}\text{Au}$ for 160 fm/c.

For a detailed comparison with experimental data we choose the system $84A$ MeV $^{12}\text{C} + ^{197}\text{Au}$ where two sets of single particle spectra are available. Figure 1 displays the density profile for a range of impact parameters in a

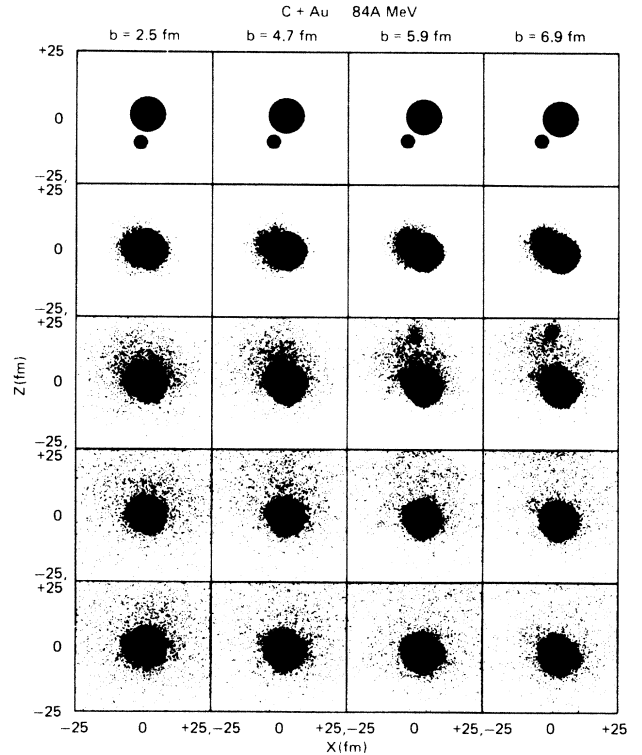


FIG. 1. Density profile of the numerical simulation of the reaction $^{12}\text{C} + ^{197}\text{Au}$ at $84A$ MeV bombarding energy. The coordinate of 100 runs are projected onto the xz plane, where z is the beam axis and x the direction of the impact parameter. For four different impact parameters ($b=2.5, 4.7, 5.9,$ and 6.9 fm) the reaction is displayed in time intervals of 40 fm/c.

sequence of time steps of 40 fm/c.

We see two well separated domains: At small impact parameters we see a complete absorption of the projectile. At large impact parameters we find a projectile remnant.

We start with the reaction at $b=2.5$ fm. At 20 fm/c the projectile nucleons have fully dived into the target nucleus. Due to collisions as well as due to the mean field the projectile spread out very fast in coordinate space. At 40 fm/c the width of the coordinate space distribution has increased by a factor of 8. Some particles have escaped, dominantly in $-x$ direction. The projectile nucleons now have a considerably higher kinetic energy (26 MeV) in their rest frame than initially. The kinetic energy of the target nucleons (21 MeV) has changed little, because the majority of them did not suffer a collision so far. However, no local temperature can be defined because the mean free path is too long compared to the dimension of the nucleus, we rather find an only weakly interacting overlay of scattered and nonscattered particles. The projectile nucleons have now lost 68% of their initial momentum. At 80 fm/c 7.1 target nucleons and 2.8 projectile nucleons are emitted. By this time almost all of them have suffered a collision and their angular distribution is far from isotropic. They carry away almost half of the available kinetic energy. With increasing time the target gets more equilibrated and the emission pattern more and more isotropic. At $b=4.7$ fm we find the system less able to spread out the projectile nucleons in coordinate space. The distance the projectile nucleons have to travel through the target nucleus decreases and gets even considerably shorter than the mean free path. However, the projectile does not survive as a cluster. While traveling through the target the mean field of the projectile pulls target nucleons along. Therefore, the shape is quite odd at 80 fm/c. At 160 fm/c equilibrium is almost established. The emission pattern is isotropic. However, less excitation energy is stored in the system, hence the number of emitted particles is lower compared to the $b=2.5$ fm reaction. At $b=5.9$ fm we see for the first time a projectile remnant of those nucleons which were initially not in the overlap of projectile and target. The density in the cluster is quite low. We expect clustering in light composites. At $b=6.9$ fm only little energy is transferred to the target. We see that a large part of the projectile survives the reaction. Also here we observe a considerable preequilibrium emission. At the end of the reaction the emission pattern is again isotropic.

Three-dimensional TDHF calculations for the same system were performed by Stöcker *et al.*¹⁶ They show qualitatively the same feature of preequilibrium emission in forward direction at low impact parameters and the surviving of a large projectile remnant at larger impact parameters. As expected the momentum transfer is larger in the BUU calculation; however, a detailed comparison is difficult because evaporation is not included in the TDHF code.

IV. DOES A HOT SUBSYSTEM EXIST?

Single particle spectra obtained in low energy reactions where a compound system is formed are exponential and

the slope parameter equals the temperature of the system. At high energy the participant spectator model, confirmed by cascade calculations, shows that only those nucleons which are in the geometrical overlap of projectile and target build a thermal source. Again the spectra are exponential but have a higher source velocity and temperature. In the medium energy regime the spectra are also exponential and consequently the slope was phenomenologically connected with a temperature of an excited subsystem which received the name hot spot. However, just from geometrical considerations the hot spot should be expected in the region where the projectile enters the target, whereas the fast particles are measured in the forward direction.

To clarify how the participant spectator model evolves from the compound model we study low impact parameter reactions at various energies. Figure 2 shows the time evolution of the reactions 25 A MeV $^{16}\text{O} + ^{197}\text{Au}$, 84 A MeV $^{12}\text{C} + ^{197}\text{Au}$, and 250 A MeV $^{16}\text{O} + ^{197}\text{Au}$ at an impact parameter of $b = 1$ fm. On the left-hand side of each plot we display the density profile of all nucleons and on the right-hand side that of the projectile nucleons only. For the 25 A MeV reaction the time interval is 80 fm/c. By 80 fm/c the projectile has crossed the target. The number of collisions having occurred by then is fairly small (65 per ensemble) because of the large Pauli blocking. But those collisions together with the mean field are effective enough to decrease the average momentum of the projectile nucleons by 80%. So the particles cannot overcome the potential barrier generated by the target nucleons. Only a few (~ 0.8 projectile and ~ 1.3 target nucleons) are able to escape, the others get reflected, and the collective velocity of the projectile nucleons is reversed. As time goes on the emission pattern gets more isotropic. By 240 fm/c, finally, the compound system is in complete equilibrium. The emission pattern is isotropic. Only a few of the projectile nucleons (~ 3) have been emitted, whereas the target has lost ~ 12 nucleons by evaporation. Mainly due to the nucleons which escaped very early in the course of the reaction and are observed at small angles do we see an anisotropy in the center of mass [$\sigma(\theta=10^\circ)/\sigma(\theta=170^\circ)=2.6$]. However, after the preequilibrium emission this reaction very much resembles a conventional compound evaporation from a source at rest in the center of mass.

The 84 A MeV reaction is displayed in a time sequence of 40 fm/c. Already by 40 fm/c we see the emission of scattered particles. By 80 fm/c when the projectile nucleons have reached the surface of the target 106 collisions have occurred. The influence of the barrier is less severe than at 25 A MeV: 2.5 projectile and 7 target nucleons escape in forward direction. Although by now many collisions are blocked the entrained nucleons proceed towards equilibration. The mechanism will be described in Sec. V. The very late stage shows once more an almost isotropic emission.

The 250 A MeV reaction, displayed in time steps of 20 fm/c, is completely different. The available phase space in nucleon-nucleon collisions is much larger and the influence of the Pauli blocking less severe. By 40 fm/c more than 200 collisions have occurred, they spread out the

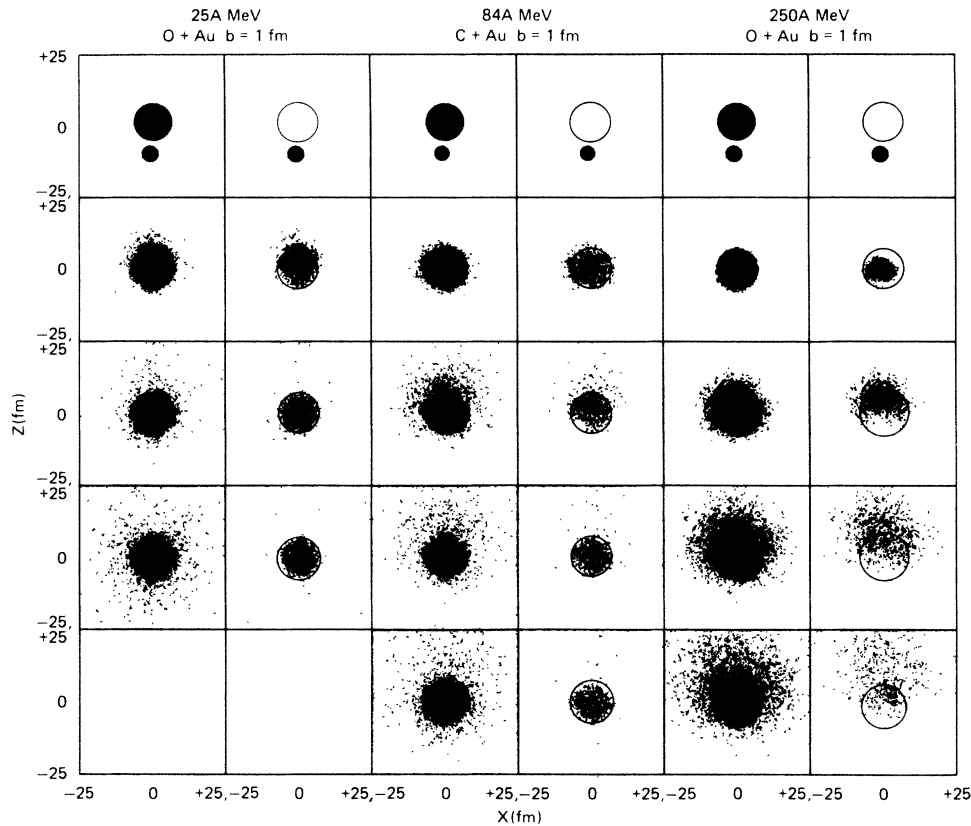


FIG. 2. Density profile of the numerical simulation of the different reactions at $b=1$ fm. The coordinates of 100 runs are projected onto the xz plane, where z is the beam axis and x is the direction of the impact parameter. The left-hand column is the projection of all nucleons, the right-hand column contains the projectile nucleons only. The position of the target is marked by the circle. The reactions are displayed in time intervals of 20, 40, and 80 fm/c for the reactions 25A MeV $^{16}\text{O} + ^{197}\text{Au}$, 84A MeV $^{12}\text{C} + ^{197}\text{Au}$, and 250A MeV $^{16}\text{O} + ^{197}\text{Au}$, respectively.

projectile nucleons in coordinate space, and knocked on many target nucleons. They reduce the average momentum of the projectile nucleons by 70%, but this is not sufficient to trap the bulk of them. Rather they escape forming a cone of roughly 90° . Also many of the knocked on target nucleons cannot be pulled back by the potential. Finally less than five projectile nucleons are in the target remnant which has lost in the average more than 20 nucleons. The evaporated particles which have almost all suffered a collision show a strong anisotropy in the center of mass system [$\sigma(\theta=10^\circ)/\sigma(\theta=170^\circ)]=6.0$.

The classical nature of the particles in the BUU approach makes it possible to trace back the particles. Therefore, we can address the question where the evaporated particles were localized at a time prior to the evaporation. This reveals whether these particles were originally localized at a certain region of the target or whether they are statistically distributed. In Fig. 3 we show the density profile at the time t_p of those particles being emitted at t_e . The location of the target is marked by a circle. We now examine the early history of those particles emitted in the reaction 25A MeV $^{16}\text{O} + ^{197}\text{Au}$. The nucleons emitted by $t_e=160$ fm/c as well as those emitted by $t_e=240$ fm/c are distributed almost statistical-

ly over the whole system at $t_p=40$ fm/c. The distribution of the emitted particles may be characterized by the second moments

$$\Delta R^2 = \sum_N (\mathbf{r}_i - \bar{\mathbf{r}})^2 / N$$

and

$$\Delta P^2 = \sum_N (\mathbf{p}_i - \bar{\mathbf{p}})^2 / N.$$

At $t=40$ fm/c we find $\Delta R^2=29$ fm², about the same as the ΔR^2 of all nucleons. So the mean field is very effective in spreading out the projectile nucleons over the whole target. Only a few (~ 20) collisions have occurred by then due to the large Pauli blocking.

The initial relative velocity between the emitted projectile and target nucleons depends on the emission time. For early emitted particles ($t_e \leq 80$ fm/c) it is 50% higher than the beam velocity V_B whereas for particles being emitted later it coincides with V_B . This can be understood as follows. A larger relative velocity results in a higher energy in the NN collisions where the available phase space is enlarged and hence the Pauli blocking less severe. This enlargement gets reduced when the system

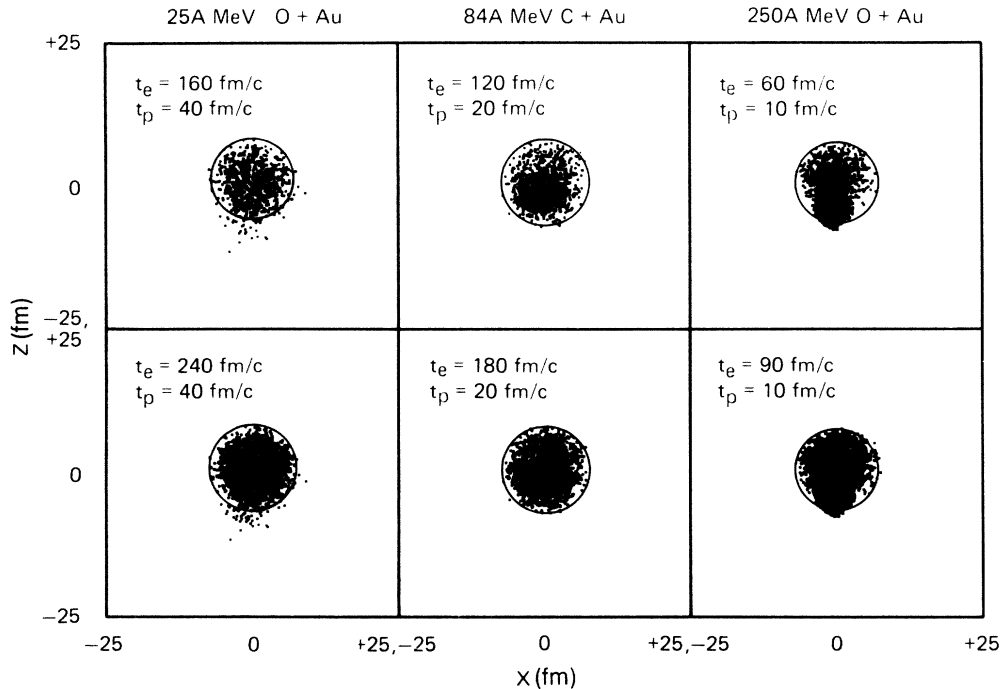


FIG. 3. Density profile of the evaporated particles. The density distribution of those particles which are emitted at time t_e is displayed at time t_p .

proceeds towards equilibrium and the phase space becomes uniformly populated. The average number of collisions of the early emitted particles ($t_e \leq 80$ fm/c) is the same as that of all projectile nucleons. The target nucleons suffered predominantly one collision. However, the projectile nucleons emitted later have suffered considerably fewer collisions than those trapped. Independent of the emission time we find an almost isotropic momentum distribution in the instant rest system but the average momentum decreases as a function of time ($\Delta P^2 = 38.6, 34.9, 32.2 \times 10^3$ (MeV) $^2/c^2$, $P_z = 71.9, 39.7, 12.2$ MeV/c for $t_e \leq 80, t_e \leq 180, t_e \leq 240$ fm/c).

The particles, which are emitted by 120 fm/c in the reaction 84A MeV $^{12}\text{C} + ^{197}\text{Au}$, show a different behavior. At 20 fm/c we see a concentration in the backward overlap region of the target ($\Delta R^2 = 21.4$ fm 2). However, the emitted particles are everywhere only a small fraction of the total particles present. When evaporated at 120 fm/c the particles have suffered ~ 2.5 collisions, however, almost all of them among one another as can be seen from the time evolution of $\bar{p}_{z, ev}$ which changes only by 15% from 40 fm/c to 120 fm/c and by the number of nucleons evaporated (\sim nine target and \sim three projectile nucleons). This can be understood as follows: Contrary to the 25A MeV reaction the Fermi spheres of projectile and target do not overlap at 84A MeV. Hence the first collisions are not limited to certain regions of the Fermi spheres. The phase space distribution proceeds much faster towards equilibrium. This increases the probability that the nucleons scatter in low momentum states and get trapped. Hence the condition to be evaporated acts as a filter for low numbers of collisions. At 120 fm/c their momentum

distribution is quite isotropic, and we find $\Delta P^2 = 49 \times 10^3$ MeV $^2/c^2$. This is almost exactly the width one expects for an equilibrated system containing three times as many target nucleons than projectile nucleons. We also find a source velocity $\bar{p}_{z, ev} = 70$ MeV/c. The particles evaporated at a later stage (between 120 and 180 fm/c) show again an isotropic distribution in the c.m. system. We find $\Delta P^2 = 30.2 \times 10^3$ MeV $^2/c^2$ and 11 times more target nucleons than from the projectile. This is consistent with a compound evaporation of a thermalized source. Also the average number of collisions increases to 3.9.

At 250A MeV we see the evaporated nucleons concentrated along the geometrical overlap of projectile and target. Compared to the 84A MeV reaction this region is more extended in z direction: the projectile nucleons can suffer much more collisions without being trapped and the effective cross section is larger because of the larger phase space available. The particles emitted by 60 fm/c have suffered ~ 5.1 collisions and have equilibrated in momentum space. $\Delta P^2 (128 \times 10^3$ MeV $^2/c^2$) is higher than expected for an equilibrated fireball, in agreement with the observation of Gutbrod *et al.*¹⁷ at central collisions of the reaction 250A MeV Ne + U. The particles emitted later show a cooler spectra ($\Delta P^2 = 50 \times 10^3$ MeV $^2/c^2$). At 90 fm/c ~ 32 particles are evaporated (1.8 as many from the target as from the projectile). $\bar{p}_{z, ev}$ falls to 60% of its value at $t = 10$ fm/c indicating that there is a lot of communication with the spectators. We find that even at 250A MeV a clear-cut between participants and spectators is not possible. However, it resembles much more this model than the reactions at lower energies.

Figure 4 shows the blocking ratio (i.e., the ratio between

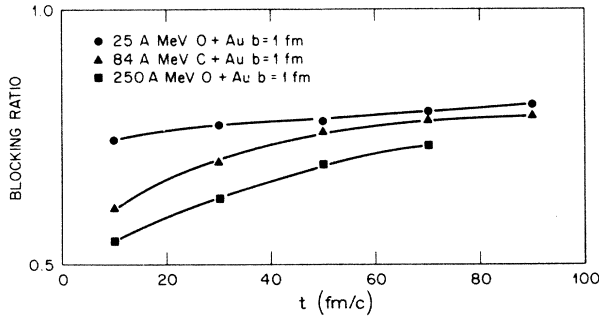


FIG. 4. Blocking ratio (i.e., number of blocked collisions/number of attempted collisions) as a function of time for the low impact parameter collision ($b=1$ fm) 25 A MeV $^{16}\text{O} + ^{197}\text{Au}$, 84 A MeV $^{12}\text{C} + ^{197}\text{Au}$, and 250 A MeV $^{16}\text{O} + ^{197}\text{Au}$.

blocked and attempted collisions) as a function of time. At the beginning we see a large energy dependence but as time goes on the ratio levels off. By that time a lot of energy is already carried away so there is only relatively cold matter left. The higher the beam energy, the higher is the energy of the early emitted particles. Hence the late stage of the reactions are similar.

Putting together now all our observations the following scenario of the reactions emerges: At 25 A MeV we see a quite large mean free path even initially. The first collision the projectile nucleons suffer is not localized. However, the mean field is strong enough to keep the nucleons together. Only a few manage to escape at the opposite surface. The bulk gets reflected and collides with further target nucleons getting more and more equilibrated. The spectrum is exponential but the slope parameter as well as the source velocity decreases as a function of the emission time.

At 84 A MeV the mean free path is considerably shorter, the source consequently more localized. However, in this case the opposite surface acts as a filter: Only those projectile particles escape which did not suffer too many collisions. The preequilibrium emission is more pronounced. It can be described as coming from a higher excited source than expected from a compound nucleus. Particles which were emitted after reflection show an increasingly lower temperature.

At 250 A MeV the mean free path is short enough to bring the overlap region close to equilibrium. However, complete equilibrium is not obtained: Finally the ratio of evaporated projectile to evaporated target nucleons is 2.8 and less than expected from a participant spectator model.

Consequently two energy domains where the emitted particles were evaporated from an almost equilibrated source are separated by an energy range where the bulk of the particles are emitted before the system approaches equilibrium. At low energy the mean field keeps the system together long enough for thermalization, at high energy the short mean free path causes the thermalization. In between the single particle spectra carry direct information of the evolution of the system towards equilibrium and offer a unique opportunity to study this approach in detail.

V. THERMALIZATION OF RESIDUAL NUCLEUS

At low energy projectile and target form a completely thermalized compound system. At high energy, on the other hand, participants form a hot thermal source and not much energy is transferred to the spectators. In between the measured single particle spectra have still an exponential form expected from a thermalized source but the slope parameters cannot be identified with a temperature of a geometrically defined subsystem. Concerning the applicability of thermal models it is important to know whether and how intermediate energy reactions lead to the thermalization of the residual nucleus. In this section we investigate in detail the approach to equilibrium in the reaction 84 A MeV $^{12}\text{C} + ^{197}\text{Au}$.

Figure 5 shows the time evolution of the density profile of projectile nucleons only. The place of the target is shown by the circle. For two impact parameters we present these plots in a time sequence of 20 fm/c. Let us first concentrate on the $b=4$ fm impact parameter. Soon after the projectile has entered the target the projectile expands in coordinate and momentum space. First, because the mean field tries to lower the density which is high in

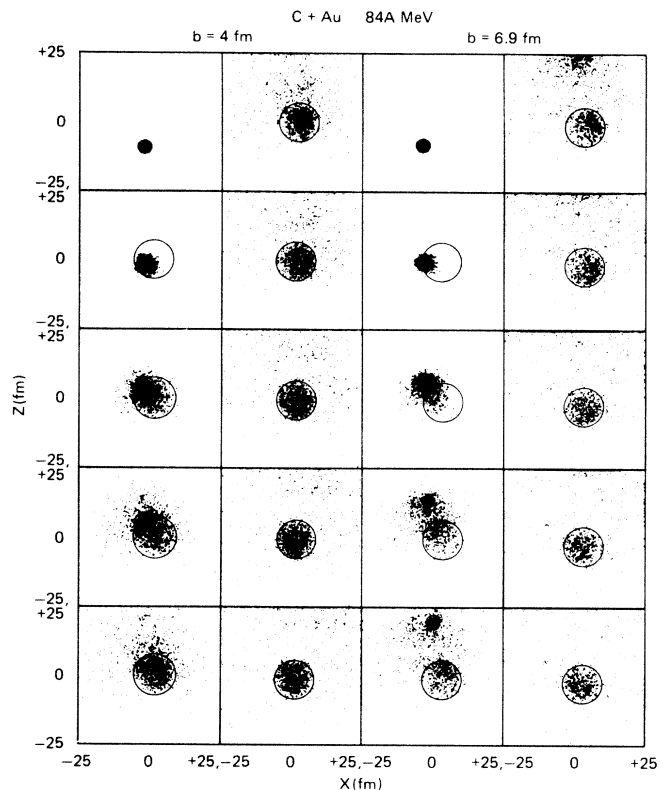


FIG. 5. Density profile of the projectile nucleons of the reaction $^{12}\text{C} + ^{197}\text{Au}$ at 84 A MeV bombarding energy. The coordinates of 100 runs were projected onto the xz plane, where z is the beam axis and x the direction of the impact parameter. For two impact parameters, $b=4$ and 6.9 fm, the nucleons are displayed in time steps of 20 fm/c. The circle marks the position of the target.

the overlap region, and second, because a number of collisions take place. The particles still have almost their initial velocity and so the Pauli blocking is less severe. At 40 fm/c some projectile nucleons have already managed to escape from the system but most have lost too much of their energy to overcome the potential barrier at the target surface. They get reflected from this wall and obtain an average momentum in $-z$ direction. By now the particles have lost sufficient energy that almost all collisions are Pauli blocked. Hence the projectile nucleons move almost freely through the interior of the target where the potential is almost constant and thus no force is acting. At 120 fm/c they have arrived at the opposite surface and once more are reflected. By 180 fm/c they are still not in complete equilibrium with the target nucleons. This phenomenon is quite independent of the impact parameter. At $b=6.9$ fm we basically see the same behavior. However, due to the larger impact parameter less projectile nucleons are trapped in the target.

To show this phenomenon from another point of view we display in Fig. 6(a) the second moments of the coordinate space (ΔR^2) and momentum space ($T = \frac{2}{3}\Delta P^2/2m$) distribution of those projectile nucleons which are trapped inside the target. These are compared with those of the target nucleons. Figure 6(b) shows the time evolution of the position of the center of mass of the trapped projectile nucleons. The numbers 1–9 mark this sequence in time steps of 20 fm/c. The full dots display the position of the center of mass of the target. At 20 fm/c we see a strong increase of T of the projectile nucleons due to the collisions. This leads to a strong spreading in coordinate

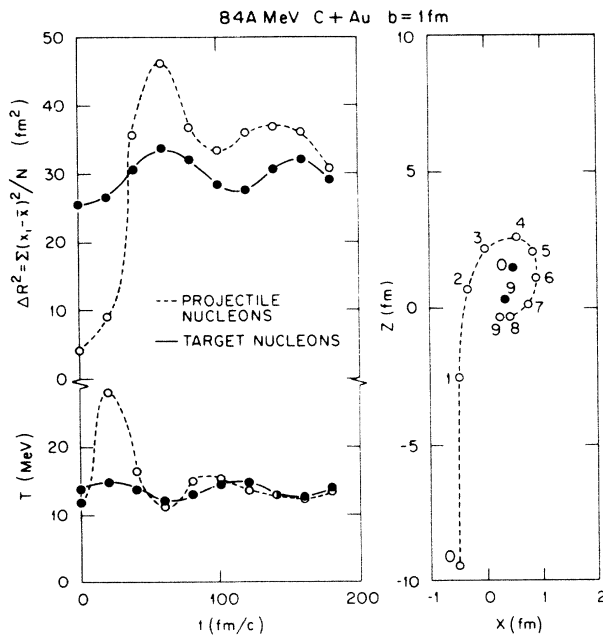


FIG. 6. Mean values X, Z and second moments ΔR^2 , $T = \frac{2}{3}(\Delta P^2/2m)$ in the rest frame of projectile and target as a function of time for the reaction 84 A MeV $^{12}\text{C} + ^{197}\text{Au}$ at $b=1$ fm. The numbers n correspond to the time n , 20 fm/c. Full dots mark the target nucleons, circles the projectile nucleons.

space and an effective deceleration in beam direction but has little influence on the target. By 80 fm/c the projectile nucleons have reached the opposite target side. They still have a considerable average velocity and try to overcome the barrier. Most of them do not succeed but stretch the combined system. This stretch causes a tension, the nucleons reverse the momentum streaming inward again. Also target nucleons enter this stressed zone and get a push inwards. This reflection also has a focusing effect in coordinate space as can be seen from Fig. 5. The additional surface tension lowers the kinetic energy. As can be seen from the momentum plot, this is the most efficient communication between target and projectile during the late stage of the reaction where almost all collisions are Pauli blocked. It causes an isoscalar vibration of the system which should be observable by γ 's of around 15 MeV. This vibration is damped but not completely washed out at 180 fm/c. At 180 fm/c the center of mass of the trapped projectile and target nucleons still do not coincide, hence a complete thermalization is not obtained by then. One word of caution should be added. Experiments show that the nucleus may fragment or undergo fission. Both are beyond our model where Coulomb energy is not incorporated and density fluctuations are washed out by the parallel run of the simulations. Both may influence the state of the system at the late stage of the reaction.

VI. EXPERIMENTAL OBSERVABLES

A. Fusion cross section

For ^{12}C projectiles on heavy targets, there is a rather well-defined impact parameter, above which a large projectile remnant is left after the collision, and below which only individual particles are emitted from the combined system. We may define fusion by the absence of a projectile fragment and find that fusion occurs with a cross section close to geometric at all energies we studied. For example, in the 84 A MeV reaction the critical impact parameter is near 5.9, and the predicted fusion cross section is 1100 mb, including the correction for Coulomb trajectories. The corresponding cross section of the 30 A MeV reaction is 1600 mb. Concerning the experimental determination of fusion, the measurements of linear momentum transfer, to be discussed later, show that there is a large fusion cross section in the sense we defined above, for energies at least up to 84 A MeV.

B. Single particle spectra

Another simple experimental observable is the single particle spectra of particles emitted from the reaction system. Usually these spectra can be described by one or more thermal sources in which the energy and momenta are shared statistically by a group of nucleons. Jakobsson¹⁰ applied a three source model to explain the data. Two of them move with the velocity of projectile and target, respectively, whereas the third one has a mid-rapidity velocity assuming a thermalized overlap region. However, because the relative velocity of projectile and

target is comparable with the Fermi velocity one does not expect such a clear cut at 84A MeV incoming energy. Figure 7 shows the theoretical proton spectra in the laboratory system compared with measurements of Jakobsson *et al.*¹⁰ In our model the proton spectrum is just half of the single particle spectra. However, some of the protons are bound in clusters. Hence we expect an overprediction of the p cross section in energy regions where clustering occurs. We see from Fig. 7 that the calculation reproduces the absolute value as well as the shape of the spectrum for angles up to 90°. However, we do not see the dip around 40 MeV but our curve is rather smooth. We overpredict the high energy tail of the 120° spectrum by a factor of 2. These particles come from the late stage of the reaction where probably a compound evaporation calculation is more suitable. Figure 8 shows the comparison with the data of Santo *et al.*¹¹ Again we get a good agreement in forward direction at high energies. In the low energy region both sets of data differ by more than a factor of 3. Again we also overpredict the backward angles. Although the high energy tails of the spectra can be approximated by an exponential, the slope parameter cannot be connected with a single temperature and the emission in the center of mass is far from being isotropic as can be seen from Fig. 9. It shows the angular distribution and the average kinetic energy of the emitted particles as a function of the emission time. At the bottom we see the center of mass distribution of those particles being emitted already at 40 fm/c. A positive angle correspond to a positive p_x component. Roughly an equal number of the emitted particles were originally projectile and target nucleons. We see a strong enhancement in forward direction

$$y = [\sigma(\theta = -10^\circ) + \sigma(\theta = 10^\circ)] / [\sigma(\theta = -170^\circ) + \sigma(\theta = 170^\circ)] = 20.$$

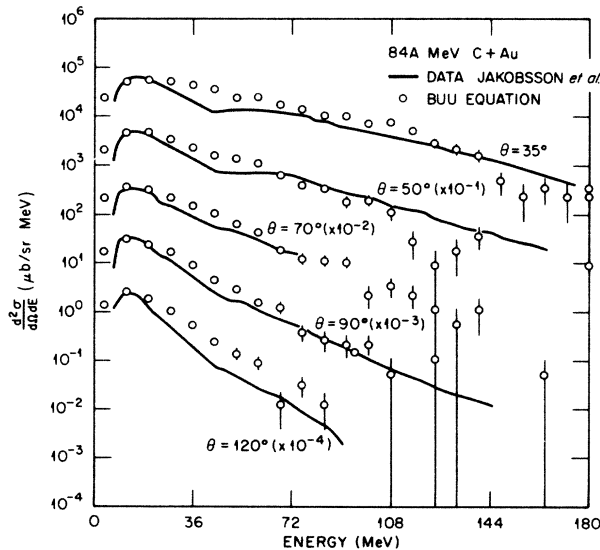


FIG. 7. The proton spectrum in the reaction $^{12}\text{C} + ^{197}\text{Au}$ at 84A MeV, comparing the theory with the results of Jakobsson *et al.* (Ref. 10). The curves show the energy at angles of 35°, 50°, 70°, 90° and 120° with curves displaced by a factor of 10 for clarity in the figure.

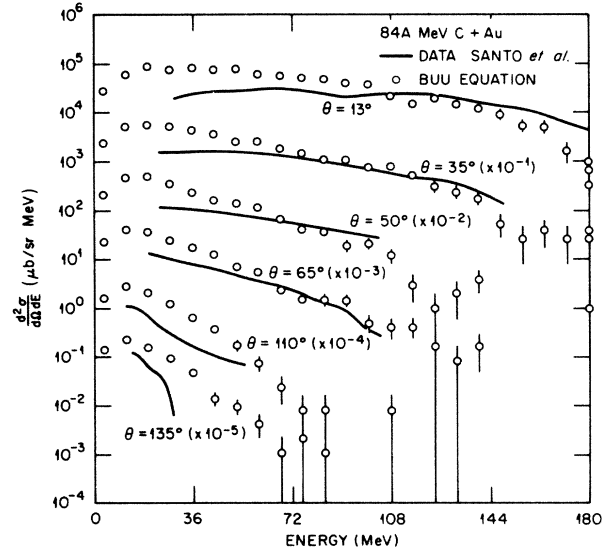


FIG. 8. The proton spectrum in the reaction $^{12}\text{C} + ^{197}\text{Au}$ at 84A MeV, comparing the theory with the results of Santo *et al.* (Ref. 11). The curves show the energy spectra at angles of 13°, 35°, 50°, 65°, 110°, and 135° with curves displaced by a factor of 10 for clarity in the figure.

The maximum is on the same side as the projectile. Most of these particles come from the hot excited subsystem described in Sec. IV. The forward emitted particles also have a much higher kinetic energy. At 120 fm/c the peak has shifted towards negative angles due to the attractive mean field. The distribution at backward angles get flatter and also the average energy is constant there. The

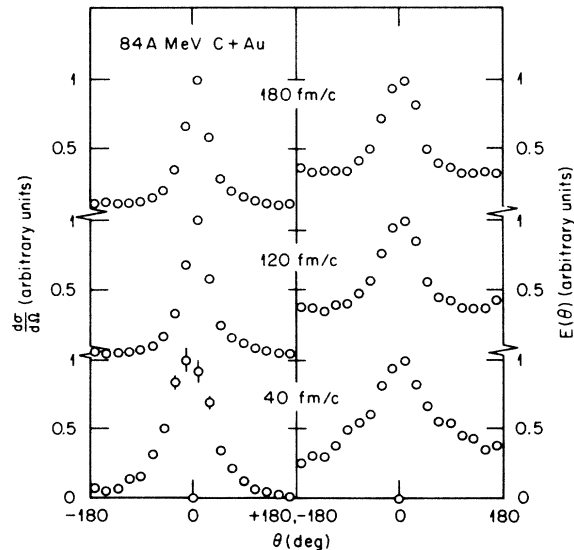


FIG. 9. Angular distribution and average kinetic energy of emitted protons as a function of time. The particles emitted during the first 40 fm/c are displayed on the bottom curve. The higher curves show the accumulated particle distribution at times $t = 120$ and 180 fm/c. Positive angles correspond to positive p_x values of the emitted particles.

final contribution at 180 fm/c still shows a distinct peak at forward direction $y=7.3$ which is associated with a larger average kinetic energy. But at backward angles $|\theta| > 90^\circ$ we find an isotropic distribution having a constant average kinetic energy. This component, which predominantly comes from the later stage of the reaction, can be identified with the evaporation from the excited target remnant. The average kinetic energy of the emitted particles decreases from 27 to 17 MeV in between 20 and 180 fm/c.

C. Multiplicity of evaporated nucleons

In high energy collisions the multiplicity serves as a measure for the impact parameter. The violent central collisions show a larger multiplicity than peripheral ones, where projectile and target almost keep their identity. At low energy we found a very small dependence of the multiplicity on the impact parameters.² There, for a large range of impact parameters a compound nucleus is formed and only a small fraction of the evaporated particles can be associated with preequilibrium evaporation.

In the reaction 84 A MeV $^{12}\text{C} + ^{197}\text{Au}$ we found an increase of the multiplicity from 13.6 at $b=8.2$ fm to 21.2 at $b=1$ fm. However, because of the limitation of our calculation to the one-body distribution function it is somewhat difficult to distinguish the evaporated particles from the projectile remnant at large impact parameters. At $b=5.9$ fm, the projectile remnant has a density less than 0.4 nuclear matter density. But the particles are very close in phase space. From a coalescence model one would expect a lot of clustering. These particles do not spoil the spectra shown in Figs. 7 and 8, but close to 0° different definitions of emission lead to different multipli-

TABLE I. Impact parameter dependence of different quantities 84 A MeV $^{12}\text{C} + ^{197}\text{Au}$. Columns a and b display the average multiplicity and target multiplicity. Column c shows the momentum transfer $x=(m_R V_R/P_{\text{proj}})$ where M_R and V_R are remnant mass and velocity, respectively. In column d we display the number of projectile nucleons which are absorbed from the target at $t=180$ fm/c. Column e shows the out of plane correlation $\sigma(\phi=7.5)/\sigma(\phi=82.5)$.

| b (fm) | a | b | c | d | e |
|--------------------------------|------|------|--------------------|-----|------|
| 1 | 21.2 | 17.5 | 0.71 | 8.3 | 1.07 |
| 2.5 | 22.1 | 17.9 | 0.66 | 7.9 | 1.23 |
| 4.0 | 21.5 | 16.7 | 0.65 | 7.1 | 1.13 |
| 4.7 | 20.8 | 15.4 | 0.56 | 6.6 | 1.22 |
| 5.4 | 20.1 | 14.1 | 0.51 | 5.9 | 1.26 |
| 5.9 | 19.9 | 13.6 | 0.56 | 5.2 | 1.43 |
| 6.4 | 17.6 | 11.5 | 0.43 | 4.8 | 1.55 |
| 6.9 | 17.1 | 10.9 | 0.41 | 4.0 | 1.27 |
| 7.4 | 14.9 | 8.9 | 0.35 | 3.1 | 1.35 |
| 7.7 | 15.1 | 8.1 | 0.35 | 2.8 | 1.51 |
| 8.2 | 13.6 | 6.9 | 0.21 | 2.0 | 1.14 |
| Impact parameter Average | 18.5 | 12.9 | 0.49 =2.3 GeV/c | | 1.29 |

cities. A better measure for the multiplicities is therefore the number of emitted particles which initially belonged to the target nucleus. Table I shows both multiplicities for a variety of impact parameters. The target multiplicity increases from 7 for the very peripheral reactions to 18 for the most central ones.

D. Linear momentum transfer

Linear momentum transfer between projectile and target may be a sensitive probe of the many-particle dynamics, as it changes most rapidly at energies where potential field effects compete strongly with nucleon-nucleon collisions. Experimentally, there are indications of systematic behavior of the momentum transfer involving both light ion and heavy ion projectiles.^{9,12,18,19} For projectiles up to ^{20}Ne , the fractional momentum transfer depends primarily on the beam velocity.⁹ At low energies, of course, the projectile transfers all its momentum and forms a compound system. The fraction decreases at higher bombarding energy, falling to about 50% at energies around 60 A MeV.¹²

From a theoretical point of view, there are several questions that arise concerning collisions with only partial momentum transfer. We would like to know the relative importance of potential field dynamics and nucleon-nucleon collisions in transferring momentum. At low energies the potential certainly is paramount in capturing the projectile to make a compound system, but the nucleon-nucleon collisions must play a major role at higher energy. We would also like to know more about the particles that carry off the remaining momentum in an incomplete fusion. In the spectator-participant picture, the momentum is associated with projectile nucleons that were outside the range of interaction with the target. Projectile particles that interact with the target may also carry off momentum if they are not sufficiently degraded in energy to be captured. The collisions exhibiting the mid-rapidity hot sources are in this category. The mechanism obviously plays a role in proton-induced reactions.¹⁹ At these reactions show, protons with energies as low as 140 MeV interact strongly enough to induce a fission but retain most of their momentum.

In our model, incomplete fusion occurs for energies about 30 A MeV. We first report the results of our model for 30 A MeV. We examined the case $^{12}\text{C} + ^{197}\text{Au}$, which was studied experimentally by Galin *et al.*¹¹ We find that there is essentially 100% linear momentum transfer for impact parameters up to 7 fm.

The momentum transfer drops precipitously at larger impact parameters, falling to 15% at $b=9$ fm. In the Galin *et al.* experiment,¹² differences were seen between an Au target and a U target, which are probably due to differences in fissibility at low excitation energy. Ignoring the uncertainties associated with this, we may say that the latter shows a strong peaking at a momentum transfer that is close to complete, $\approx 85-95\%$. It is not clear to us whether there is a significant difference from our findings.

The results at higher energy are completely different. For the reaction $^{12}\text{C} + ^{197}\text{Au}$ at 84 A MeV we find that

even in central collisions the momentum transfer is not complete. We define $x = M_R V_R / P_{\text{proj}}$ as a measure for the momentum transfer where M_R and V_R are the remnant mass and velocity, respectively. For a complete momentum transfer $x = 1$. The values for different impact parameters are displayed in Table I. For the most central collision ($b = 1$ fm) $x = 0.71$. Also at this low impact parameter collision, where almost all projectile particles have suffered at least one collision, we see a significant preequilibrium emission before the system gets thermalized. The nucleus is no longer transparent for the bulk part of the projectile nucleons as we saw for $84A$ MeV $^{12}\text{C} + ^{12}\text{C}$,¹ but it is also not extended enough to equilibrate the system completely. The momentum transfer gets less complete with increasing impact parameters. As long as the projectile dives fully into the target this is due to the decreasing extension of the target in Z direction. For larger impact parameters it is due to a projectile leftover. Averaging over impact parameters we find a mean momentum transfer of 2.3 GeV/ c . The distribution $P(x)$ of the transferred momentum is displayed in Fig. 10. This value agrees very well with the measured momentum transfer.¹² The number of projectile nucleons which have fused are also displayed in Table I. At $b = 1$ fm 8.3 projectile nucleons are finally in the target, more than two have already escaped by 60 fm/ c , whereas the thermalized rest gets evaporated during the later step of the reaction. Even at the largest impact parameter ($b = 8.2$) there are still two projectile nucleons entrained in the compound system.

Figure 11 shows the distribution of the transferred momentum in comparison with the data of Galin *et al.*¹² for the reaction $60A$ MeV $^{12}\text{C} + ^{197}\text{Au}$. The absolute magnitude is adjusted by eye and we assume an energy independent fissibility. The calculation agrees with the experimental finding that already at $60A$ MeV the momentum transfer is by far not complete. The calculated width coincides with the data; the calculated maximum is

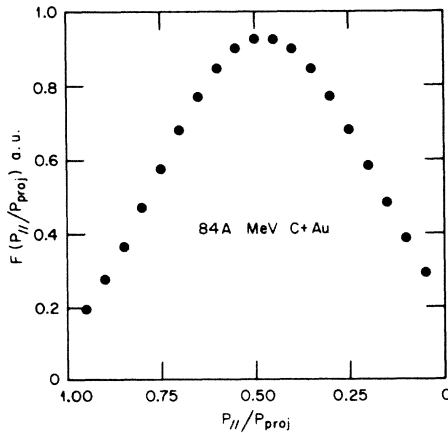


FIG. 10. Distribution of the momentum transfer $P(x)$ summed over all impact parameters for the reaction $84A$ MeV $^{12}\text{C} + ^{197}\text{Au}$.

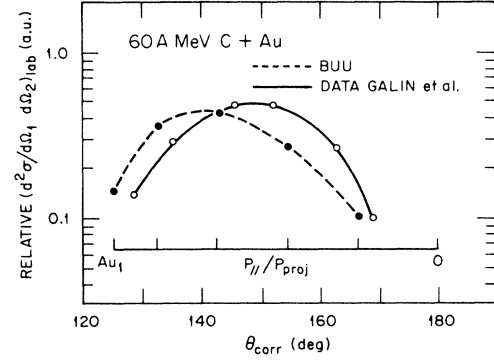


FIG. 11. Distribution of the linear momentum transfer for the reaction $^{12}\text{C} + ^{197}\text{Au}$ at $60A$ MeV. The full line shows the result of Galin *et al.* (Ref. 12), the dotted line is our prediction.

around 70% of the total momentum whereas the measurements show a maximum at around 55%. The difference may be due to physical reasons. The large momentum transfer at small impact parameters is associated with a high excitation energy of the system. So the system may breakup in many fragments instead of fissioning.

This is supported by the analysis of the multifragmentation process which at this energy shows a center of mass velocity⁶ of the fragmenting system which is close to the expected compound nucleus velocity. So further experiments would certainly be helpful to investigate both mechanisms in more detail.

Momentum may be transferred by two-body collisions and the mean field. If two-body collisions dominate we expect a linear dependence of the momentum transfer on the diameter of the system. Figure 12 shows the momentum transfer for low impact parameter reactions $84A$ MeV $^{12}\text{C} + A$ and $44A$ MeV $^{40}\text{Ar} + A$. We first discuss the carbon-induced reaction. For large targets we see indeed a momentum transfer proportional to $A^{1/3}$. For small targets ($A \leq 27$), however, the momentum transfer drops faster. Here the mean free path is about the size of

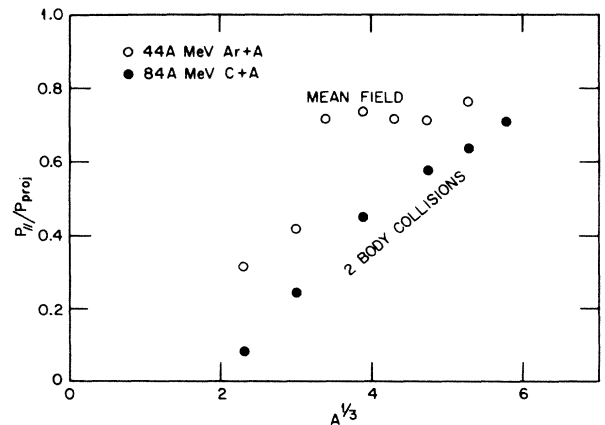


FIG. 12. Linear momentum transfer as a function of the target mass for the reactions $84A$ MeV $^{12}\text{C} + A$ and $44A$ MeV $^{40}\text{Ar} + A$.

the system, hence only few collisions take place. These collisions are not very effective in transferring momentum. Nucleons which scatter have a high probability to be emitted before sharing their momentum with other nucleons. The mean field acts very similar to neighboring nucleons. For that reason the projectile and target nucleons, which do not suffer a two-body scattering, stay together and emerge as a cluster. For a detailed discussion of the momentum transfer and its implication on the mean free path we refer to Ref. 20. The 44 A MeV reactions show a completely different behavior. We see a pronounced structure of the momentum transfer. It reaches a local maximum around $A=60$ and is smaller for larger targets. The underlying mechanism can be seen from Fig. 13. For targets smaller than $A=60$ we see two remnants, whereas for larger targets a combined system is found. Around $A=60$ there are not enough collisions to disperse the projectile but enough to deaccelerate it considerably. The bulk of the projectile nucleons cannot overcome the potential barrier at the opposite side of the target. A very prolate system emerges before the mean field restores a spherical shape. This collective deacceleration caused by the mean field is very effective in transferring momentum and allows only few nucleons to escape before having shared their momentum.

E. Azimuthal correlations

Another observable of our calculation is the out of plane correlation. By our setup we define a reaction plane and can study the polar angle dependence of the emission probability. The out of plane correlation of light particles emitted in the reaction 25 A MeV $^{16}\text{O} + ^{197}\text{Au}$ was measured by Lynch *et al.*¹³ searching for particle emission from a hot subsystem. The data show an inplane enhancement

$$0.5 \times [\sigma(\phi=0^\circ) + \sigma(\phi=180^\circ)] / \sigma(\phi=90^\circ) = 1.5$$

and a small asymmetry around $\phi=90^\circ$ as a consequence of the momentum conservation. This asymmetry does not

show up in our model because the total momentum of the 100 simulations is conserved, but not the momentum of each individual simulation. Our model predicts an out of plane correlation of

$$\sigma(\phi=7.5^\circ) / \sigma(\phi=82.5^\circ) = 1.4 \quad (1.3)$$

for 30 (84 A) MeV $^{12}\text{C} + ^{197}\text{Au}$. We also find that the higher the kinetic energy of a particle the higher the probability of being emitted on the side opposite to the projectile. This agrees with recent experimental findings.²¹

VII. CONCLUSIONS

Our study of heavy systems with the Boltzmann-Uehling-Uhlenbeck model corroborates the usefulness of this approach for investigating the dynamics of heavy ion reactions. The theory predicts the single particle observables well. In the reaction 84 A MeV $^{12}\text{C} + ^{197}\text{Au}$ we find a good agreement between the calculated single particle distribution and the experimental proton cross section. The single particle distribution shows two components: An early preequilibrium emission in forward direction of those nucleons which have crossed the target without getting thermalized, and an almost isotropic emission of the late particles emitted after a compound system is established. The model is also able to reproduce quantitatively the distribution of momentum transfer between 30 A and 84 A MeV as well as the out of plane correlations at 30 A MeV.

Neither a 84 A MeV ^{12}C projectile nor a 44 A MeV ^{40}Ar projectile can be stopped by any of the investigated targets, even in very central collisions. The increasing mean free path as a function of the number of collisions enables some nucleons to escape before an equilibrium is established. Thus incomplete fusion is not a geometrical effect caused by the incomplete overlap of projectile and target. For small targets remnants of projectile and target survive. In reactions with large projectiles and moderate beam energies the deacceleration is dominated by the

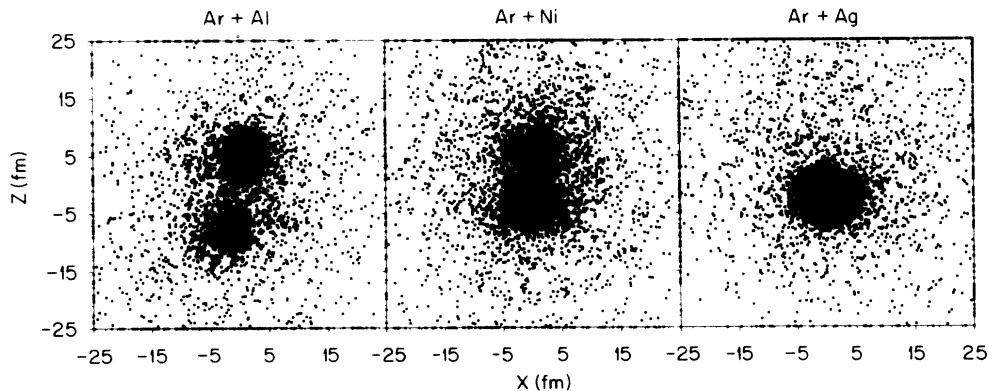


FIG. 13. Density profile of the reactions $^{40}\text{Ar} + ^{27}\text{Al}$, $^{40}\text{Ar} + ^{58}\text{Ni}$, and $^{40}\text{Ar} + ^{107}\text{Ag}$ at 44 A MeV bombarding energy and $t=180$ fm/c. The coordinates of 100 runs were projected onto the xz plane, where z is the beam axis and x the direction of the impact parameter.

mean field, for heavier targets and higher beam energies collisions are dominant. They disperse the projectile nucleons and consequently no projectile remnants are found.

Those projectile nucleons which finally are absorbed by the target do not get equilibrated on their way through the target. Two-body collisions, suppressed by the Pauli blocking, are not effective enough to spread them over the available phase space. Rather they get reflected by the potential well on the opposite side of the target causing a vibration of the system which is not completely damped at $180 \text{ fm}/c$.

The question whether there exists a hot thermalized region where all the early evaporated particles originate from turns out to be more difficult to answer than assumed in the phenomenological models. At $25 A \text{ MeV}$ we find a quite large region due to the large mean free path. At $84 A \text{ MeV}$ this region is more localized in coordinate space. However, this region is dominantly occupied by particles which are not evaporated and which did not suffer a collision. A local equilibrium is not established. Both findings rule out a hydrodynamical approach to these reactions. The spectrum of the early emitted parti-

cles is exponential and the slope is angle independent in the rest frame of the source. However, the source velocity as well as the slope parameter changes considerably as a function of the emission time.

At $250 A \text{ MeV}$ we find that the geometrically overlapping zone forms the source of particle emission. The small nucleon-nucleon mean free path brings this zone close to equilibrium but the slope of the momentum distribution is angle dependent. The source contains less target nucleons than expected from the participant spectator model.

ACKNOWLEDGMENTS

We want to thank G. Bertsch for many stimulating discussions and helpful suggestions as well as S. Umar and J. Maruhn for helping us to adjust the computer programs to the FPS computer. This work was supported in part by the National Science Foundation under Grant PHY84-13287 and the Department of Energy under Grant DE-AC05-84OR21400.

*Present address: Institut für Theoretische Physik, Philosophenweg 19, D-6900 Heidelberg, Federal Republic of Germany.

¹The Boltzmann-Uehling-Uhlenbeck equation is first given in E. A. Uehling and G. E. Uhlenbeck, *Phys. Rev.* **43**, 552 (1933). This method has been applied to nuclear collisions at various levels of sophistication by several authors, e.g., B. Remaud, F. Seville, C. Gregoire, and F. Scheuter, *Nucl. Phys.* **A428**, 101 (1984); C. Gregoire and F. Scheuter, *Phys. Rev. Lett.* **146B**, 21 (1984); W. Cassing, Gesellschaft für Schwerionenforschung Report 84-15, 1984; C. Toepffer and C. Y. Wong, *Phys. Rev. C* **25**, 1018 (1982); C. Gregoire, B. Remaud, F. Scheuter, and F. Seville, *Nucl. Phys.* **A436**, 365 (1985). The present three-dimensional approach was first applied at high energy: G. F. Bertsch, H. Kruse, and S. Das Gupta, *Phys. Rev. C* **29**, 673 (1984); H. Kruse, B. V. Jacak, and H. Stöcker, *Phys. Rev. Lett.* **54**, 289 (1985).

²J. Aichelin and G. Bertsch, *Phys. Rev. C* **31**, 1730 (1985). A very similar approach (called VUU approach) was advanced by H. Kruse, B. V. Jacak, J. J. Molitoris, G. D. Westfall, and H. Stöcker, *Phys. Rev. C* **31**, 1770 (1985).

³W. G. Lynch *et al.*, *Phys. Rev. Lett.* **51**, 1850 (1983).

⁴J. Aichelin, *Phys. Rev. Lett.* **52**, 2343 (1984).

⁵D. J. Fields *et al.*, *Phys. Rev. C* **30**, 1912 (1984).

⁶J. Aichelin, J. Huefner, and R. Ibarra, *Phys. Rev. C* **30**, 107 (1984).

⁷W. A. Friedman and W. G. Lynch, *Phys. Rev. C* **28**, 16 (1983).

⁸A. D. Panagiotou *et al.*, *Phys. Rev. C* **31**, 55 (1985).

⁹G. La Rama *et al.*, *Nucl. Phys.* **A407**, 233 (1983).

¹⁰B. Jakobsson *et al.*, Proceedings of the 4th Bergen Workshop on Nuclear Physics, 1982; A. Oskarsson, Lund University Report 8303, 1983.

¹¹R. Santo *et al.*, Gesellschaft Für Schwerionenforschung Annual Report, 1984.

¹²J. Galin *et al.*, *Phys. Rev. Lett.* **48**, 1787 (1982).

¹³M. B. Tsang *et al.*, *Phys. Lett.* **148B**, 265 (1984).

¹⁴H. Mori, *Prog. Theor. Phys.* **8**, 327 (1952).

¹⁵L. P. Kadanoff and G. Baym, *Quantum Statistical Mechanics* (Benjamin, Reading, Mass., 1962).

¹⁶H. Stöcker, R. Y. Cusson, J. A. Maruhn, and W. Greiner, *Phys. Lett.* **101B**, 379 (1981).

¹⁷Gutbrod *et al.*, *Nucl. Phys.* **A387**, 177c (1982).

¹⁸V. E. Viola *et al.*, *Phys. Rev. C* **26**, 178 (1982).

¹⁹F. Saint-Laurent *et al.*, *Nucl. Phys.* **A422**, 307 (1984).

²⁰J. Aichelin and H. Stöcker, *Phys. Lett.* **163B**, 59 (1985).

²¹G. Caskey *et al.*, *Phys. Rev. C* **31**, 1597 (1985).